Effect of phosphorus dopant on photoluminescence and field-emission characteristics of Mg 0.1 Zn 0.9 O nanowires

Chia Ying Lee, Tseung Yuen Tseng, Seu Yi Li, and Pang Lin

Citation: Journal of Applied Physics **99**, 024303 (2006); doi: 10.1063/1.2161420
View online: http://dx.doi.org/10.1063/1.2161420
View Table of Contents: http://scitation.aip.org/content/aip/journal/jap/99/2?ver=pdfcov
Published by the AIP Publishing

Effect of phosphorus dopant on photoluminescence and field-emission characteristics of $Mg_{0.1}Zn_{0.9}O$ nanowires

Chia Ying Lee
Department of Electronics Engineering and Institute of Electronics, National Chiao Tung University, Hsinchu 300, Taiwan

Tseung Yuen Tseng[a)]
Department of Electronics Engineering and Institute of Electronics, National Chiao Tung University, Hsinchu 300, Taiwan and Department of Materials and Mineral Resources Engineering, National Taipei University of Technology, Taipei 106, Taiwan

Seu Yi Li and Pang Lin
Institute of Materials Science and Engineering, National Chiao Tung University, Hsinchu 300, Taiwan

(Received 24 May 2005; accepted 29 November 2005; published online 20 January 2006)

The photoluminescence and field-emission properties of $Mg_{0.1}Zn_{0.9}O$ nanowires (MZO NWs) hydrothermally grown on the *p*-type silicon (100) substrates with and without phosphorus dopant were investigated in this study. Parts of MZO NWs were treated with PH_3 plasma to form phosphorus-doped MZO NWs (PMZO NWs). The MZO and PMZO are wurtzite single crystals, and the surface morphologies of MZO NWs are identical to those of PMZO NWs with an average diameter of 50 nm and a length of 500 nm. The direct band gaps and emitted ultraviolet photoluminescences of the MZO and PMZO NWs are 3.41 eV and 403.8 nm and 3.56 eV and 385.4 nm, respectively. The MZO NWs grown on Si substrates have an emission threshold electric field of 1.8 $V/\mu m$ (current density of 1.0 mA/cm^2) and a field enhancement factor, β, of 3048 while the PMZO NWs show enhanced properties with a threshold electric field of 1.5 $V/\mu m$ and a β value of 3054. These field-emission properties are also enhanced by illumination, which reveals that the emission behavior is affected by the surface charge state. Therefore, it is suggested that the band structure of MZO NWs has been modulated by phosphorus incorporation. © *2006 American Institute of Physics*. [DOI: 10.1063/1.2161420]

I. INTRODUCTION

Recently, one-dimensional nanowires (NWs) have been extensively studied for potential applications to photonic, electro-optical, and electronic devices because of their unique physical and chemical properties. There are various methods to synthesize the NWs; however, the hydrothermal process has several advantages over other growth processes such as catalyst-free growth, low cost, large area uniform production, environmental friendliness, and low reaction temperature to integrate into the microelectronics and plastic electronics. The NWs with sharp tips are suitable structures for cold cathode field-emission device application. It has been reported that the emission characteristics of Si NWs depend on the doping type (*n* and *p* types).[1–3] However, the field-emission properties of other NWs with various dopants are still unclear.

Zinc oxide (ZnO) is an attractive material for electronic and electro-optical devices, such as the ultraviolet (UV) laser device,phosphor, transparent conducting films for solar cell, and flat panel display, because of its wide band gap (3.4 eV) and large exciton binding energy (60 meV).[4–6] Current trends in developing ZnO-based optoelectronic devices are focused on synthesizing reliable *n*-type and *p*-type ZnO.[7,8] But, it was difficult to fabricate reproducible *p*-type ZnO due to self-compensation and low solubility of dopants.[9] Recently, Norton and co-workers have reported that the $P_{0.02}Mg_{0.1}Zn_{0.9}O$ film showed stable *p*-type behavior by adding Mg and P together—Mg dopant to increase the band gap and P dopant to introduce the acceptor level.[10,11]

In this work, the $Mg_{0.1}Zn_{0.9}O$ (MZO) NWs are fabricated on *p*-type [B doped, 1–10 Ω cm] Si substrates by the hydrothermal method. The P ions were incorporated into part of the MZO NWs to form phosphorus-doped MZO NWs (PMZO NWs) by using plasma treatment. The crystal structure, chemical composition, photoluminescence, and field-emission characteristics of MZO and PMZO NWs on the *p*-type Si (100) substrates were examined. The effect of phosphorus dopant on the properties of MZO NWs was also studied.

II. EXPERIMENT

Before deposition, the *p*-type Si substrates were cleaned by Radio Corporation of America (RCA) clean process to remove native silicon oxide on the substrate surface. Ultrathin ZnO seeding film (~70 Å) was deposited on the Si substrate by rf-sputtering (13.56 MHz) method under Ar sputtering gas at 20 mTorr. Then, the coated Si substrate was put into an aqueous solution (Milli Q, 18.2 MΩ cm) of zinc nitrate hexahydrate ($Zn(NO_3)_2 \cdot 6H_2O, 0.01M$), magnesium nitrate hexahydrate ($Mg(NO_3)_2 \cdot 6H_2O, 0.06M$), and diethylenetriamine (HMTA, $C_6H_{12}N_4$) with a *p*H value

[a)]Author to whom correspondence should be addressed; electronic mail: tseng@cc.nctu.edu.tw

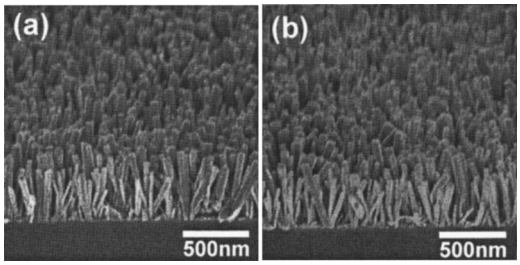

FIG. 1. Cross-section FESEM micrographs of (a) MZO NWs, and (b) PMZO NWs grown on Si substrates.

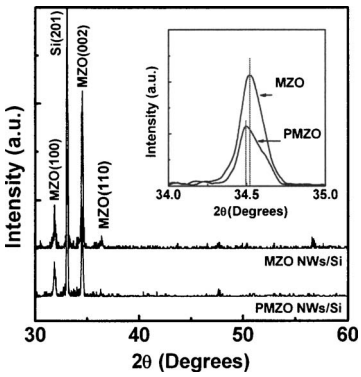

FIG. 2. XRD patterns of (a) MZO NWs and (b) PMZO NWs grown on Si substrates. The inset is the enlarged patterns with 2θ from 34° to 35°.

of 7.2 in a sealed vessel at 75 °C for 1 h. After this hydrothermal reaction, the MZO NWs can be formed on the Si substrate and the color of the product was gray. The microstructure and properties of the synthesized MZO NWs that have been cleaned with deionized (DI) water and dried in the vacuum oven at room temperature for 5 h were investigated. To fabricate the PMZO NWs, the MZO NWs were exposed to PH_3 plasma for 120 s. The plasma treatment was carried out in an inductively coupled plasma (ICP) reactor using a 3 kW ICP power supply. The processing conditions were under 10 mTorr working pressure, 200 W ICP, 200 °C reaction temperature, and both Ar (99.5%) and PH_3 (99.5%) with 100 cm^3/min flow rate. Then, these NWs were rapid thermally annealed (RTA) at 300 °C for 30 min in the oxygen atmosphere. The crystal structure of the NWs was examined by x-ray diffraction (XRD) (MAC Science, MXP18, Japan). The surface morphologies of the NWs were observed by field-emission scanning electron microscopy (FESEM) (Hitachi S-4700I, Japan) and high-resolution transmission electron microscopy (HRTEM) (Philips tecani–20). The chemical composition of the NWs was analyzed by x-ray photoelectron spectroscopy (XPS) (VG Scientific ESCALAB 250). Room-temperature optical properties characterizations were performed by UV-visible (UV-VIS) spectrometer Hitachi 557, Japan) and photoluminescence analyzer (PL, Hitachi F–4500, Japan) with Xe lamp as an excitation source (325 nm). The conducting behaviors of MZO and PMZO were characterized by the Hall-effect measurements (HL500PC) at a magnetic-field strength of 0.3 T at room temperature. The samples used for this measurement were bulk materials, which have the same chemical compositions as the NWs. The field-emission characteristics of the NWs were measured by Keithley 237 source-measure unit in a vacuum chamber at a pressure of 1×10^{-6} Torr at room temperature. In the field-emission measurement, a tungsten anode with an area of 7.0×10^{-3} cm^2 was placed at a distance of 350 μm from tips of the NWs, which can be adjusted by a precision screw meter with an accuracy of ±0.1 μm.

III. RESULTS AND DISCUSSION

The typical FESEM images which illustrate the surface morphologies of MZO and PMZO NWs on *p*-type Si substrates are shown in Fig. 1. It is indicated that the randomly oriented MZO NWs have an average diameter of 50 nm, an average length of 0.5 μm, and a number density of 3.4×10^{10} cm^{-2}. These NWs are nonvertical and randomly distributed over the polycrystalline ZnO seeding film and exhibit homogeneous morphologies with hexagonal columnar shape. The surface morphologies of PMZO NWs [Fig. 1(b)] including shape, diameter, length, and number density are identical to those of MZO NWs. Thus, the surface morphologies of the MZO NWs remain unchanged after the PH_3 plasma treatment.

The crystal structure and phase of the NWs were determined by XRD. Figure 2 depicts the XRD patterns of MZO and PMZO NWs grown on the *p*-type Si substrates, respectively, and the inset is the enlarged XRD patterns of peak (002) of the NWs with 2θ from 34° to 35°. The XRD peak at 33.06° is caused by the Si substrate, and three main diffraction peaks are indexed as (100), (002), and (110) of the wurtzite structure, respectively. Thus, single phase MZO and PMZO NWs with the wurtzite structure were synthesized by the hydrothermal method. The lattice constants and corresponding cell volumes ($3\sqrt{3}a^2c/2$) of MZO and PMZO NWs can be calculated from their XRD patterns. The *c*-axis lengths calculated from the (002) peak of MZO and PMZO are 5.192 and 5.198 Å, respectively; *a*-axis length calculated from the (100) peak is 3.241 Å for both NWs, and the cell volumes are 141.69 and 141.86 $Å^3$, respectively. After the P plasma treatment, the PMZO NWs retain the crystal structure of wurtzite and no other impurities appear but have a small change in the *c*-axis length and slight increase in cell volume. The variation of the *c*-lattice constant may be due to the P plasma implanting perpendicularly to the substrate. Such a P implantation along the (002) direction of MZO leads to an increase in the *c*-axis parameter. The addition of P to MZO forms a solid solution with the wurtzite structure; a possible reaction is

$$P''' \xrightarrow{\text{(Mg,Zn)O}} P'_{\text{O}} + V''_{\text{(Mg,Zn)}}, \tag{1}$$

where P'_{O} means P^{3-} substituted for O^{2-} site and $V''_{\text{(Mg,Zn)}}$ indicates a vacancy formed at a Zn^{2+} or Mg^{2+} site in the lattice of the MZO NWs. It is suggested that a P^{3-} ion is substituted for an O^{2-} ion, which leads to a Zn vacancy formation. Therefore, the deviation of the lattice constants can be due to the P atoms incorporated in the NWs by plasma implantation and the different ionic radii between P^{3-} (r_{P}^{3-} = 1.06 Å) and O^{2-} (r_{O}^{2-} = 0.73 Å).

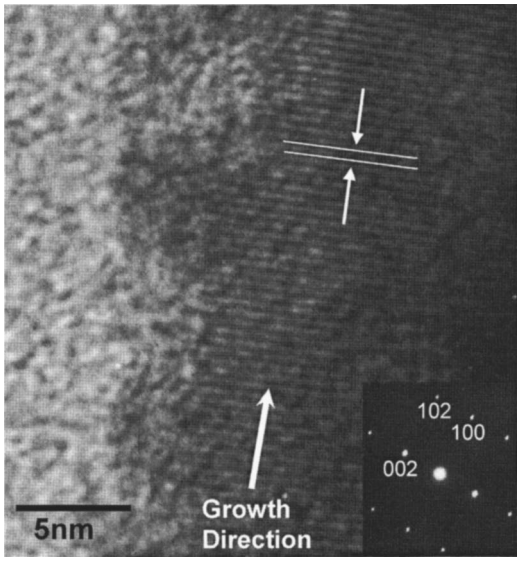

FIG. 3. HRTEM micrograph of PMZO NWs. The inset is the corresponding SAED of the NWs.

The typical HRTEM image of PMZO NWs and corresponding selected area electron diffraction (SAED) are shown in Fig. 3, which illustrates the microstructural features of the PMZO NWs. The SAED pattern in the inset of Fig. 3 can be indexed to the reflection of single-crystalline PMZO hexagonal structure, and its lattice constants are $a=b=3.241$ Å and $c=5.198$ Å, which are consistent with the XRD result. The SAED pattern indicates that the NWs grow in the [0002] direction with wurtzite structure, and the distance between parallel [0002] lattice fringes of the NWs is 5.198 Å. This pattern also depicts the single-crystalline structure of the PMZO NWs. Moreover, the defects such as dislocations and stacking fault were not observed in the PMZO NWs. For both the MZO and PMZO NWs, only the growth direction [0002] was found. It concludes that the MZO NWs can be doped with P by the plasma treatment but without damaging its crystal structure.

The chemical composition of the PMZO NWs was further analyzed by the XPS and the results are shown in Fig. 4. The XPS spectrum of PMZO NWs shows that there are feature peaks corresponding to elements of Zn, Mg, P, O, C, and Si. Three strong peaks located at 530.8, 1024.4, and 1048.0 eV are, respectively, due to the O ($1s$) and Zn ($2p_{3/2}$ and $2p_{1/2}$) binding energies for ZnO NWs, while three weak peaks located at 49.6, 129.9, and 130.5 eV are due to the Mg ($2p$) and P ($2p_{3/2}$ and $2p_{1/2}$) binding energies for Mg and P incorporated in the NWs. The appearance of carbon at the peak of 263 eV results from the residual reactants adsorbed on the surface of the NWs, and the peak of Si was detected due to the Si substrate. Obviously, the dominant chemical composition of the NWs is ZnO and a little amount of Mg and P is incorporated into these NWs on the basis of the results of XPS measurement. With further detailed examinations, the chemical composition of these NWs is $P_{0.02}Mg_{0.1}Zn_{0.9}O$.

Figure 5(a) shows the photoluminescence spectra of MZO and PMZO NWs excited by a Xe lamp ($\lambda=325$ nm) at

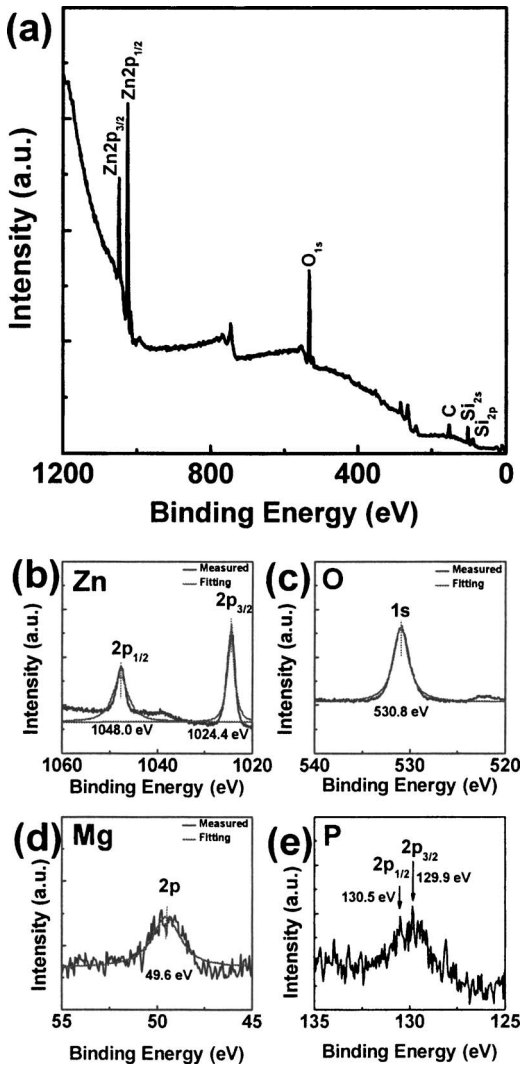

FIG. 4. (a) XPS spectrum of PMZO NWs, (b) Zn spectrum, (c) O spectrum, (d) Mg spectrum, and (e) P spectrum.

room temperature. It is indicated that MZO NWs emit luminescences at 403.8 nm (3.07 eV), 451 nm (2.75 eV), 465 nm (2.67 eV), 495 nm (2.51 eV), and 520 nm (2.38 eV), respectively. The UV emission at 403.8 nm is caused by the band-edge emission of MZO. The luminescence at 451 nm was reported to be due to the Zn vacancy (V''_{Zn}).[12] The emission of 465 nm may be associated with the oxygen deficiency in these NWs formed in the growth environment of hydrothermal process.[13] The possible reactions that take place in the aqueous solution in such an environment are the following:

$$(CH_2)_6N_4 + 10H_2O \rightarrow NH_4OH + 6HCHO, \quad (2)$$

$$(Zn^{2+}, Mg^{2+}) + 2OH^- \rightarrow (Zn,Mg)O + H_2O. \quad (3)$$

The Zn^{2+} ions are sufficient in this solution, but the OH^- ions are finite in the solution because hexamethylenetetramine (HMTA) slowly releases OH^-. Thus, oxygen is expected to be lacking in the NWs fabricated by the hydrothermal method. This phenomenon also results in the deep-level[14] and singly ionized oxygen vacancies[15] luminescences at 495 and 520 nm as shown in Fig. 5(a). On the other

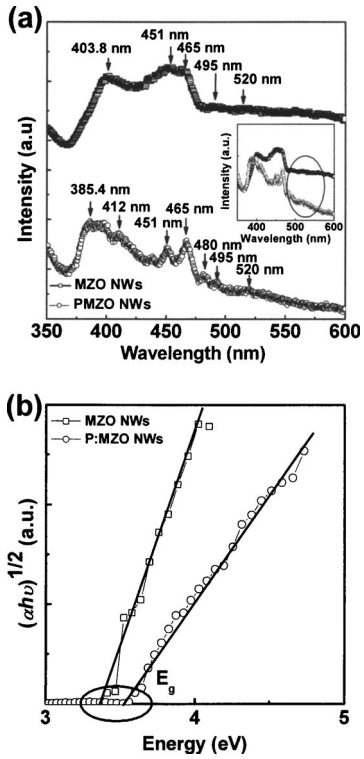

FIG. 5. (a) Photoluminescence (PL) spectra of MZO and PMZO NWs. (b) Tauc's plots of MZO and PMZO NWs.

hand, the PMZO NWs emit 385.4 nm (3.22 eV), 412 nm (3.02 eV), 451, 465, 480 nm (2.58 eV), 495, and 520 nm luminescences. It is shown that the near band-edge emission peak shifts from 403.8 to 385.4 nm and a Stokes shift of 0.15 eV happens as the P was incorporated in the MZO NWs. Such a blueshift of optical band-to-band transitions was reported to be related to the Burstein-Moss effect.[16] The emissions at 412 and 480 nm may be associated with the nonstoichiometric oxide[17] and ionized Zn vacancy (V'_{Zn}) (Ref. 12) in the PMZO NWs. The UV emission of PMZO NWs is a little weaker than that of MZO NWs, while the emissions of PMZO NWs at 465, 495, and 520 nm caused by oxygen vacancies are much weaker than those of MZO NWs. It could be proposed that the P substitution causes the oxygen vacancies in PMZO to decrease and introduces an acceptor level leading to a decrease in electron concentration but an increase in hole concentration and finally PMZO NWs become *p*-type conduction, which can be further verified by the following the Hall-effect measurement. Room-temperature transmission spectra of MZO and PMZO NWs were recorded by an UV-visible spectrometer. To realize the relationship between the transmission spectra and the band gap, $(\alpha h\nu)^{1/2}$ is plotted as a function of photon energy ($h\nu$) as shown in Fig. 5(b). The absorption edge is used to determine the energy band gap (E_g) of the NWs. The band gap of MZO NWs is 3.41 eV, and that increases to 3.56 eV for the PMZO NWs. Such an increase is attributed to the broadening effect[18] occurring as the carriers feel different potentials for the different local concentrations of the substituting elements in the crystal. Therefore, the band gap can be modulated by adding P content in the MZO NWs, which may be applied in various optoelectronic applications.

On the basis of the results of the Hall-effect measurement, the MZO bulk performs the *n*-type conduction with a resistivity of 1.1 Ω cm, Hall mobility of 10.2 cm^2/V s, and carrier concentration of 5.8×10^{17} cm^3, while the PMZO one exhibits the *p*-type behavior with a resistivity of 4.3×10^{-1} Ω cm, Hall mobility of 15.8 cm^2/V s, and carrier concentration of 9.2×10^{17} cm^3. Therefore, it can be expected that the PMZO NWs also exhibit *p*-type conductivity due to the same composition between NWs and bulk materials we measured.

The field-emission characteristics of the MZO and PMZO NWs on the *p*-type Si (100) substrate are shown in Fig. 6. As shown in Fig. 6(a), the turn-on electric field (E_{on}, under the current density of 1.0 $\mu A/cm^2$) and threshold electric field (E_{th}, under the current density of 1.0 mA/cm^2) of MZO NWs are 1.3 and 1.9 $V/\mu m$, respectively, while those of PMZO NWs are 1.0 and 1.5 $V/\mu m$, respectively. The semilogarithmic plots of *J-E* field-emission characteristics shown in the inset of Fig. 6(a) further identify their emission properties. These plots can be divided into three parts: zero emission (region 1), Fowler-Nordheim (F-N) field emission (region 2), and current saturation region (region 3). The E_{on} is defined as the electric field for which tunneling of PMZO NWs occurs and is 1.0 $V/\mu m$ which is lower than that of MZO NWs (1.3 $V/\mu m$). Above E_{on} (region 2), the emission current density abruptly increases and then saturates at the high electric-field region (region 3). The current density emitted by MZO NWs is lower than that of PMZO NWs under the same electric field. A knee electric field, E_{knee}, is defined as the demarcation point between F-N field-emission and current saturation regions. The E_{knee} of MZO and PMZO NWs, respectively, are 1.8 and 1.5 $V/\mu m$. In this F-N tunneling region, the better field-emission properties were observed for the PMZO as compared with MZO because the resistance of PMZO is smaller. This worse field-emission ability of MZO may be due to a potential barrier formed by the negative charge in the surface state of *n*-type emitters.[1,2] Thus, the *p*-type PMZO NWs with lower surface state barrier perform the better field-emission properties. The MZO and PMZO NWs on *p*-type Si substrates perform at a saturation region at higher electric field (region 3) in the *J-E* plot. This saturation region exists due to the high resistance in the series of semiconductor emitters.[19] As shown in the inset of Fig. 6(a), the resistances in series of MZO and PMZO NWs are introduced to fit the *J-E* plot and the values of 93 and 62 kΩ are obtained, respectively. The decreasing resistance in the series of PMZO NWs is attributed to a lower potential barrier formed by the positive charge in the surface state of *p*-type PMZO emitters. Obviously, the P dopant can improve the field-emission properties of MZO NWs on the *p*-type Si (100) substrate. The PMZO NWs with the low threshold electric field and low resistance in series are suitable for the field-emission applications.

The corresponding F-N plots [$\ln(J/E^2)$ vs E^{-1}] of the MZO and PMZO NWs on the *p*-type Si (100) substrate are

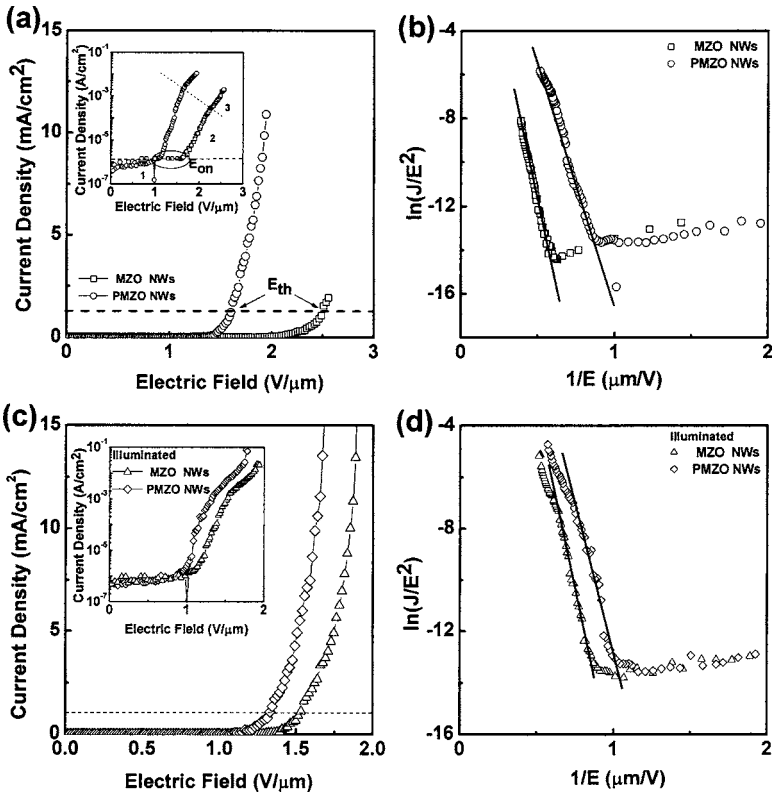

FIG. 6. (a) Field-emission *J-E* curves of MZO and PMZO NWs grown on *p*-type Si substrate. The inset is the semilogarithmic *J-E* plot and resistance in series fitting. (b) The corresponding F-N $[\ln(J/E^2)$ vs $E^{-1}]$ plots of the NWs. (c) Photoenhanced field-emission characteristics of MZO and PMZO NWs grown on Si substrates. The insert is the fitting of resistance in series. (d) Corresponding F-N plots.

depicted in Fig. 6(b), indicating that the measured field-emission characteristics fit the F-N relationship. The F-N relationship is as follows:

$$J = \frac{A\beta^2 E^2}{\phi}\exp\left(\frac{-B\phi^{3/2}}{\beta E}\right), \tag{4}$$

where J is the current density, E the applied field, Φ the work function of the ZnO (5.37 eV), β the field enhancement factor, $A=1.56\times10^{-10}$ (A V^{-2} eV), and $B=6.83\times10^{3}$ (V $eV^{-3/2}$ μm^{-1}). The calculated β value of MZO NWs is 3048, and that of PMZO NWs is 3054. Therefore, the β value of PMZO NWs is close to that of MZO NWs. It is well known that the β depends on the geometry, structure, tip size, and number density of the emitters on the substrate. It is believed that the similar surface morphology and structure between PMZO and MZO NWs (Figs. 1–3) is the main reason for having nearly same β values.

The photoenhanced field-emission properties of MZO and PMZO under a 30 W incandescent lamp irradiation are studied to demonstrate the influence of the illumination on the field emission. The E_{on}, E_{th}, E_{knee}, β, and R_s values of these NWs can be obtained from the slopes and fitting curves of the F-N plots and are listed in Table I. The E_{on} and E_{th} of PMZO NWs under illumination decrease to 0.9 and 1.3 V/μm, respectively, and its maximum current density increases to 72 mA/cm^2. As shown in the insert of Fig. 6(c), the calculated resistances in series of the MZO and PMZO NWs under illumination from the fitting are 72 and 45 kΩ, respectively, which are lower than those values without illumination. The β values of these two NWs under illumination calculated from the slopes of the F-N plots [Fig. 6(d)] are identical to those of the dark one. Therefore, it is demonstrated that the carriers in the MZO and PMZO NWs are excited during the illumination, leading to an increase in the emission current density and a reduction in the resistance in series, but unchanged structure and surface morphology after illumination lead to similar β values.

Figure 7 depicts the *J-E* curves and corresponding F-N plots with E from 0 to 1.95 V/μm (forward sweep) and then back to 0 V/μm (backward sweep) of PMZO NWs grown on the *p*-type Si substrate. The two *J-E* curves are almost merged and no hysteresis behavior caused by adsorbates[20] is

TABLE I. E_{on}, E_{th}, E_{knee}, β, and R_s values of MZO NWs and PMZO NWs grown on the Si substrates with and without illumination.

	MZO		PMZO	
	Dark	Illuminated	Dark	Illuminated
E_{on} (V/μm)	1.3	1.0	1.0	0.9
E_{th} (V/μm)	1.9	1.5	1.5	1.3
E_{knee} (V/μm)	1.8	1.6	1.5	1.4
β	3048	3049	3054	3058
R_s (kΩ)	93	72	62	45

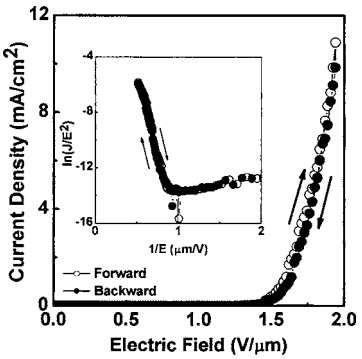

FIG. 7. Field-emission *J-E* curves of PMZO NWs with forward and backward sweeps. The inset depicts the corresponding F-N plot.

observed in this measurement. Thus, it is demonstrated that the good field-emission performance (low turn on electric field and high emission current density) of PMZO NWs is not caused by the adsorbates on the NWs but the intrinsic properties of the NWs.

IV. CONCLUSIONS

In summary, the single-crystalline MZO and PMZO NWs on the *p*-type Si (100) substrates are synthesized by hydrothermal route. The structure and surface morphology of MZO NWs are similar to those of PMZO NWs. The average diameter of these two nanostructures is 50 nm and the length is 500 nm. Room-temperature transmission spectra illustrated that the band gap of MZO NWs shifts from 3.41 to 3.56 eV, and the band-edge emission from 403.8 to 385.4 nm when the plasma implantation of P into them occurs to form PMZO NWs. Moreover, such PMZO NWs exhibit better field-emission properties including the lower threshold electric field, lower resistance in series, and higher emission current density, in comparison with MZO NWs. The improved field-emission characteristic of PMZO is attributed to the changes in surface state of the nanostructure at both threshold voltage and F-N field-emission regions. The PMZO NWs with good field-emission properties are a suitable material for flat display application. Moreover, the modulated band gap can be obtained with P doping but keep similar crystal structure, which may also be able to be applied for the future nanohomojunction ZnO optoelectronic and field-emission devices.

ACKNOWLEDGMENT

This work was supported by the National Science Council of R.O.C. under Contract No. NSC 93–2216–E–009–024.

[1]S. Johnson, A. Markwitz, M. Rudolphi, H. Baumann, S. P. Oei, B. K. Teo, and W. I. Milne, Appl. Phys. Lett. **85**, 3277 (2004).
[2]T. Matsukawa, S. Kanemaru, K. Tokunaga, and J. Itoh, J. Vac. Sci. Technol. B **18**, 1111 (2000).
[3]S. Kanemuru, T. Hirano, H. Tanoue, and J. Itoh, Appl. Surf. Sci. **111**, 218 (1997).
[4]S. Y. Li, P. Lin, C. Y. Lee, and T. Y. Tseng, J. Appl. Phys. **95**, 3711 (2004).
[5]A. Gupta and A. D. Compaan, Appl. Phys. Lett. **85**, 684 (2004).
[6]S. Fujihara, A. Suzuki, and T. Kimura, J. Appl. Phys. **94**, 2411 (2003).
[7]J. M. Bian, X. M. Li, C. Y. Zhang, W. D. Yu, and X. D. Gao, Appl. Phys. Lett. **85**, 4070 (2004).
[8]K. Ip, Y. W. Heo, D. P. Norton, S. J. Pearton, J. R. LaRoche, and F. Ren, Appl. Phys. Lett. **85**, 1169 (2004).
[9]S. B. Zhang, S. H. Wei, and Y. Yan, Physica B **302**, 135 (2001).
[10]Y. K. Kwon, Y. Li, Y. W. Heo, M. Jones, P. H. Holloway, D. P. Norton, Z. V. Park, and S. Li, Appl. Phys. Lett. **84**, 2685 (2004).
[11]Y. W. Heo, Y. K. Kwon, Y. Li, S. J. Pearton, and D. P. Norton, Appl. Phys. Lett. **84**, 3474 (2004).
[12]S. A. M. Lima, F. A. Sigoli, M. Jafelicci, Jr., and M. R. Davolos, Int. J. Inorg. Mater. **3**, 749 (2001).
[13]Y. Du, W. L. Cai, C. M. Mo, J. Chen, L. D. Zhang, and X. G. Zhu, Appl. Phys. Lett. **74**, 2951 (1999).
[14]J. Wang, G. Du, Y. Zhang, B. Zhao, X. Yang, and D. Liu, J. Cryst. Growth **263**, 269 (2004).
[15]K. Vanheuseden, W. L. Warren, C. H. Seager, D. R. Tallant, J. A. Voigt, and B. E. Gnade, J. Appl. Phys. **79**, 7983 (1996).
[16]T. Makino, Y. Segawa, S. Yoshida, A. Tsukazaki, A. Ohtomo, and M. Kawasaki, Appl. Phys. Lett. **85**, 759 (2004).
[17]S. S. Chang, S. O. Yoon, H. J. Park, and A. Sakai, Mater. Lett. **53**, 432 (2002).
[18]R. D. Shannon, Acta Crystallogr., Sect. A: Cryst. Phys., Diffr., Theor. Gen. Crystallogr. **32**, 145 (1976).
[19]S. Y. Li, P. Lin, C. Y. Lee, T. Y. Tseng, and C. J. Huang, J. Phys. D **37**, 2274 (2004)
[20]H. Z. Zhang, R. M. Wang, and Y. W. Zhu, J. Appl. Phys. **96**, 624 (2004).